

GROUND-BASED OPTICAL POSITION MEASUREMENTS OF SPACE DEBRIS IN LOW EARTH ORBITS

D. Hampf, W. Riede, G. Stöckle, I. Buske
DLR, Institute of Technical Physics, 70569 Stuttgart, Germany

Abstract

The increasing amount of space debris requires the satellite operators to handle a growing number of collision risk assessments in order to eventually perform collision avoidance manoeuvres. For this scheme to work effective and reliable, the acquisition of highly accurate orbital position data of detected threatening space debris is necessary.

The successful experimental demonstration of our earlier published concept on laser-based distance measurements of space debris in low earth orbits has proven this technique to be feasible for this task. Hereby a powerful short pulse laser system within a ground-based transceiver set-up is used to measure the time-of-flight of the back-scattered laser pulse from the space debris object. The time-of-flight information ultimately correlates with the object distance.

A passive optical tracking unit equipped with a highly sensitive camera system is used for initial localisation and coarse determination of the debris position to guide the laser towards its target. In addition this unit provides the capability to determine accurate angular position information using the recorded star background.

To experimentally investigate the potential contribution of a passive optical tracking unit for the debris position determination and to further develop our proposed concept, we have installed a passive-optical station at the public observatory on the Uhlandshöhe in Stuttgart. We will discuss the requirements and the technical difficulties to set up such a system. Thereby we highlight the system parameters which influence the measurement accuracy as well as the debris size threshold. Furthermore we will give an outlook on our planned developments for the future.

1 INTRODUCTION

The space-flights conducted since the mid of the 20th century have resulted in a type of environmental pollution which is not usually addressed in discussions about sustainability, but may become a serious problem in the near and mid-term future: Space debris. Summarised under this term are leftovers from all sorts of activities in space, mainly in earth orbits of different heights. Typical objects include defunct satellites, rocket bodies and boosters and fragments thereof, which may be produced by mechanical break-ups, explosions or collisions. At low earth orbits, up to a few hundred kilometres, debris objects are decelerated by the residual atmosphere, which eventually results in a re-entry into the atmosphere and a decrease of the amount of space debris in orbit. At higher altitudes, however, in-orbit times range from decades (around 600 to 800 km) to centuries (above 800 km) [17].

The most crowded orbits today are the LEO (low earth orbit, up to 2,000 km altitude) and GEO (geostationary orbit, about 36,000 km altitude). Within the LEO, objects cluster especially around altitudes of 800

to 1,000 km [12]. At these altitudes, the risk of a collision between a debris object and an active spacecraft is not negligible. Since there are different popular inclinations among the orbits, large impact angles may occur, and relative velocities of colliding bodies can exceed 10 km/s [17]. Dedicated observation schemes are in operation world-wide to detect debris objects and record their orbits. For example, the US Space Surveillance Network maintains several radar and optical telescopes that continuously monitor objects in space, the majority of which are space debris. The resulting data is used (among other things) for real-time risk assessment, and warnings are issued to satellite operators in case of an impending collision.

The results are partly available to the public, e.g. through the SATCOM catalogue [8]. By mid 2013, the catalogue contains almost 17,000 objects, of which 13,000 are classified as debris. The current survey capabilities are limited to objects above a size of about 10 cm. It is estimated that there are about 700,000 debris objects in LEO with sizes greater than 1 cm [22].

Currently, most observations of debris in LEO are conducted using radar facilities [17]. There are, however, also plans for an increased use of optical obser-

vations for this task. This seems especially promising if the passive optical observations are coupled with an active channel for laser ranging, as explained in section 2 of this paper. In section 3 a new experiment is described, which is currently being installed at the observatory of Stuttgart with the goal to test and demonstrate the capability of active optical space debris observations. In sections 4 and 5 the planned measurements and some first results are presented.

2 OPTICAL MEASUREMENTS OF SPACE DEBRIS

2.1 Passive optical observations

Passive optical observations can be used both to detect new space debris particles as well as to track and further characterise the objects. This scheme uses the fact that orbital objects are illuminated by the sun and reflect part of the sunlight to the observer on the ground. The objects appear as quickly moving spots against the fixed star background.

As noted already in the introduction, observations of space debris in LEO are today usually conducted by radar facilities, while optical observations are mostly used for observation of objects at GEO altitudes. There are, however, notable exceptions: For example, the Magdalena Ridge Observatory [16] in New Mexico, USA, is used for precise tracking of previously discovered objects and their characterisation, e.g. by recording of light curves (which translate into information about the object rotation). There have also been simulation studies indicating that a network of optical sensors can reach the same performance as a radar network concerning object discovery and determination of orbital parameters [11].

A main caveat of optical observations is a problem well-known also in astronomy: From the observations alone it is not possible to deduce the object's distance, or its altitude above the ground. This factor constitutes the main source of error in the calculation of the orbital parameters. One possible solution might be the simultaneous observation of the same target from different sites [18]. Another option is the measurement of the object distance by means of laser ranging, which will be introduced in the following subsection.

2.2 Active optical observations

In contrast to the passive optical observations, where the object is illuminated by the sun, active optical observations require the illumination of the object by a strong, pulsed laser beam (sender channel). With a sensitive detector (receiver channel) the returning light pulses can be measured and correlated to the pulses sent by the laser. The time difference between the

pulse emission from the laser and the detection of the returning pulse provides a direct measurement of the distance between the observer and the targeted object (laser ranging) [6, 20, 23].

While this method alone cannot detect new objects, it can be used to determine orbital parameters of previously detected objects with much greater accuracy and with fewer measurements (which in turn increases the potential of the system to record more objects per time interval). Typically a space debris observation system would combine a passive channel for the initial detection of the object and its tracking, and a laser ranging unit to determine the distance.

For a number of satellites, laser ranging is routinely employed to obtain precision data on their orbits (satellite laser ranging, SLR, [7]). While the technology is similar to active optical debris observations, there are some significant differences: First, the orbits of the satellites used for SLR are very well known beforehand. Therefore, the satellites can be targeted using orbital parameters alone, and SLR stations do not need a passive optical channel to track or even detect objects. Second, the expected return time of the light pulse is very well defined due to the known orbit, and the receiver can be gated to a very narrow time window, thus minimising the noise. Third, the satellites targeted by SLR stations are equipped with retro-reflectors which project a significant amount of light back to the light source, while space debris will usually only produce diffuse reflection. On the other hand, the time resolution usually aimed at is in the picosecond regime in order to achieve accuracies of mm in the distance measurements, which are needed for the objectives of typical SLR applications but not for space debris observations. Nevertheless, the technology and the experience available at SLR stations can be a guide for the development of facilities for the active optical space debris observations.

So far, laser ranging to space debris objects has only been successfully attempted by few projects: In Australia, the EOS Space Debris Tracking System uses a 100 W Nd:YAG laser and a 1.8 m telescope to track objects down to 10 cm size [19], successfully demonstrating the power of this technique. In Europe, the DLR Stuttgart and the SLR station Graz have tracked a number of un-cooperative objects (i.e. not equipped with retro-reflectors) during a test campaign in 2012. Using a 1 kHz Nd:YAG laser with 10 ns pulse duration and 25 mJ pulse energy, the distances to objects in LEO could be measured with accuracies better than 1 meter [9].

3 EXPERIMENTAL SET-UP

To further develop the concept of active optical measurements an experimental system is currently being



Figure 1: The experimental set-up at the Stuttgart observatory as of June 2013.

installed at the public observatory of Stuttgart. The final system will consist of a passive optical channel used to detect and track objects, and an active optical channel used for laser ranging.

A first version of the passive optical channel has seen first light on April 14th, 2013. Currently, hard- and software of the system are tested and developed further. In particular, different configurations, e.g. different cameras, filters or additional optical components, are tested to achieve the best possible performance. Apart from that, the system is being upgraded to automatise as many functions as possible and to increase the system accuracy and reliability. The installation of the active optical path is foreseen for 2014 and 2015.

3.1 Infrastructure

Since the main objective of the installation will be the test and demonstration of new technologies rather than routine observations of orbital objects, a good infrastructure and accessibility has been given precedence over observing quality during the site selection. The public observatory in Stuttgart¹ has proven to be the ideal place for this. Located in the heart of Stuttgart, about 20 minutes by car from the institute and only a short walk from the city's main station, it allows for an efficient installation process and unconstrained experimenting time. A non-profit society maintains regular amateur astronomical observations and public outreach activities at the site and offers invaluable assistance in the set-up and tuning of the instruments.

The observatory is located at 48° 47' 00.26" N, 9° 11' 50.91" E at an altitude of 351 meters above sea level. The experiment is located on the roof of the main building, protected by an Astrohaven clamshell dome with a diameter of 3.6 m and a height of about 3

¹Schwäbische Sternwarte, <http://www.sternwarte.de/>

Total aperture	432 mm
Corrected aperture	396 mm
Focal plane Ø	52 mm
Focal length	2939 mm
Focal ratio	$f/6.8$

Table 1: Specifications of the Planewave CDK 17" telescope used for the experimental set-up [13].

Slewing speed	20° / s
Acceleration	20° / s ²
Absolute pointing accuracy	< 5 arcsec
Sidereal tracking accuracy	< 1 arcsec

Table 2: Specifications of the Astelco NTM-500 mount [2].

m (Fig. 1). Apart from about 10 degrees in azimuth towards north, where the view is blocked by another part of the building, the location provides an unobstructed view into all directions down to the horizon. The equipment can be controlled either from within the dome, or from a workstation in the main building while monitoring the interior of the dome with a surveillance camera.

The drawbacks of the site are the poor weather conditions typical of north western Europe, and a relatively high level of light pollution from the city. The latter point is mitigated, however, by the fact that the view towards south east (which is the best direction for satellite viewing in the evening hours) is directly away from the city centre and towards sparsely populated areas of the mountains surrounding the city (see section 5.2 for first measurements of the light pollution).

3.2 Passive optical channel

For the passive optical channel a 17" (43 cm) PlaneWave Corrected Dall Kirkham telescope [13] is used (see table 1 for the specifications). It is mounted on an equatorial Astelco NTM-500 mount, which offers a fully computerised control with high pointing accuracy and short slewing times (see table 2).

Two different focal plane arrays are available for recording images from the telescope:

- Finger Lakes Instruments (FLI), ProLine 16803: A CCD astrocamera with a large chip (and therefore field of view) and high resolution.
- Andor, iXon DU 897 Ultra: An emCCD camera with a smaller chip, high sensitivity and a high frame rate.

Table 3 summarises the most important specifications of the two cameras. All observations presented in section 5 have been conducted using the FLI camera. First tests using the Andor iXon camera are foreseen for the coming months.

	FLI PL	iXon
Field of view [°]	0.7	0.16
Resolution [pixels]	4096 x 4096	512 x 512
Pixel size [μm]	9	16
Scale [arcsec / pixel]	0.63	1.12
Integration time [s]	0.02	0.01
RO time [s]	2.1	~ 0
RO noise [e ⁻ / pix]	9	0.4 (equiv.)
dark noise [e ⁻ / pix / s]	0.07	0.001

Table 3: Specifications of the two cameras available for passive optical observations. The field of view and the scale are only valid for the described set-up using the CDK 17" telescope. The integration times refer to shortest possible exposures, and all values refer to full resolution mode [4, 1, 14].



Figure 2: The passive optical set-up as of July 2013. The main telescope is the Planewave CDK 17" described in the text, the two smaller telescopes are so far only used for calibration and tests. The light from the main telescope is recorded by an FLI ProLine camera equipped with a 7-slot filter wheel.

To further optimise the performance of the system, wavelength filters can be inserted into the optical path. The possible benefit for the operations that can be achieved, e.g. by filtering out typical wavelengths induced by man-made light pollution, will be investigated. Additionally, a focal reducer can be inserted to increase the field of view at the expense of the resolution. Figure 2 shows the passive optical set-up as of July 2013.

3.3 Active optical channel

The active optical channel is currently in its design phase. The goal is to test, tune, characterise and demonstrate a system to measure distances to orbital objects using laser ranging. The system will consist of a sender channel, i.e. a pulsed laser, and a receiver channel, i.e. a sensitive photon detector.

The laser envisaged for the first tests should have a pulse rate of about 1 kHz and a pulse energy of a few ten mJ. While this will suffice for the principle test of laser ranging in our facility, it should be emphasised that for detecting smaller debris particles stronger lasers are needed, which are under development [5]. From our calculations it seems that a Yb:YAG laser used at its fundamental wavelength of 1030 nm may be well suited for this application [21]. Since it is not feasible to install such a strong laser onto a fast telescope mount, the laser will remain stationary and the laser beam will be guided via a mirror system onto the target.

The detector must be sensitive to single photons in the desired laser wavelength range. In principle, silicon and InGaAs avalanche photodiodes are promising candidates for wavelengths in the near-infrared. Various commercial detector modules are currently being evaluated. In parallel, the optical path of the passive optical channel is being modified to couple out some light at the laser wavelength and guide it onto the detector.

The read-out electronics must register the exact time between the emission of the laser pulse and the signal of the returning photons. For this, a PicoQuant TimeHarp 260 module is foreseen. Additionally, the system will need to gate the detector to the anticipated arrival time of the photons in order to suppress noise. This is a non-trivial feature, since it requires an a-priori knowledge of the object distance. It is currently foreseen to use a custom FPGA module for this task. If the dead-time of the detector and the readout system is acceptable, it may also be possible to register all photon signals and to evaluate the signals off-line with variable assumptions about the object distance.

4 OBSERVATION MODES

This section introduces the observation modes that are implemented or planned at our observatory. The tracking modes 'Leap Frog Tracking' and 'Continuous tracking', which are described in subsections 4.1 and 4.2, can both be used for tracking objects with known orbits (subsection 4.3) and objects without known orbits (subsection 4.4).

4.1 Leap Frog Tracking

In this mode, the software calculates the position where the searched-for object is expected to be a few seconds later (5 to 15 seconds have been found to work well for our system). The telescope then slews to this position and holds there. At the exact point in time when the object is expected to cross the field of view, the camera starts a short exposure (typically between 0.05 and 0.4 seconds for our current configuration). In

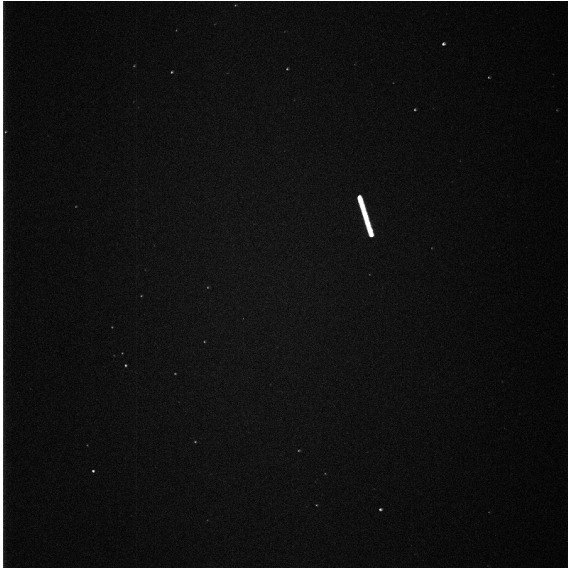


Figure 3: Image recorded with the described set-up (FLI-camera) on April 14th, 2013. The arc is produced by the bright track of satellite Resurs DK-1, a Russian science vessel approximately 3 x 8 x 10 metres in size. Apart from the arc about 30 stars are visible, albeit much weaker than the track imprinted by the satellite. The exposure time is 0.1 seconds, the pixel binning is 2.

the resulting image the stars appear as points while the tracked object produces an arc, whose length is determined by the angular velocity of the object and the exposure time. Figure 3 shows an image recorded in this mode.

The analysis of such an image yields the coordinates of the satellite at the beginning and end of the exposure time. The exact pointing of the telescope can be derived from the stars visible in the field of view by referencing with a star catalogue. The satellite coordinates can be inferred subsequently taking into account the transformation matrix between camera coordinates and astrometric coordinates. To break the ambiguity between start and end of the track, the flight direction must be known (can be inferred from the position of the previous or subsequent image). During a typical pass of an object, several dozen images can be recorded, which can subsequently be used to derive the orbital parameters.

For this mode, the telescope can be operated in a fairly ordinary fashion (using standard go-to commands as used for astronomical observations). The camera, however, must be triggered with high temporal accuracy, since the satellite moves through the field of view in less than a second (towards zenith, an object in LEO has an angular velocity of about 1° per second).

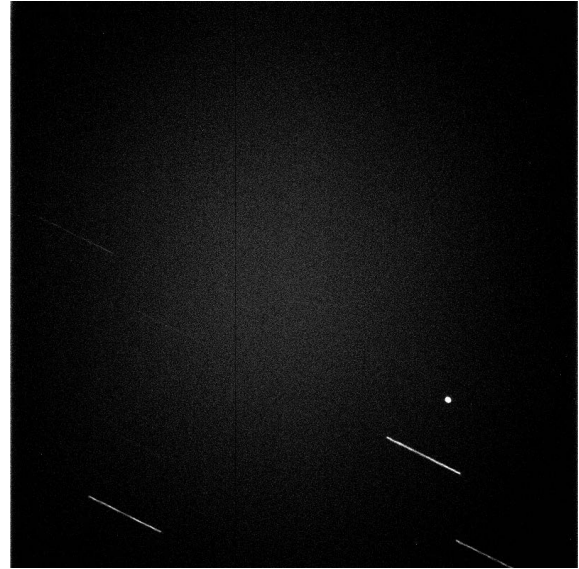


Figure 4: Image taken while tracking satellite SL-8 (satellite number 03230) on 2013-07-11 at 22:06 UTC. The satellite appears as bright point in the lower right corner. A few stars are visible as arcs. The exposure time is 0.5 seconds, the pixel binning is set to 3.

4.2 Continuous Tracking

In this mode, the telescope is constantly moving to keep the object continuously within the field of view. Images can be taken at any time, relaxing the demand of exact camera triggering. However, for the later evaluation of the images and the calculation of orbital parameters the recording times of the images must be accurately known. Images taken in this mode show the object as small point (in case of perfect tracking the size of the point is only determined by the quality of the optics, the seeing and possibly the non-negligible extension of the object) and the stars as arcs. The determination of the astrometric position requires the reduction of these arcs to their start or end points. In figure 4 an example of an image recorded in this mode is shown.

While a pure passive optical determination of object orbits can make use of either leap-frog or continuous tracking, the combination with an active optical channel requires the use of the latter to keep both the sender and the receiver continuously on target.

4.3 Tracking objects with known orbital parameters

For the test of a new system it is convenient to track known, bright objects. But also in actual debris monitoring there is a need for this observation mode: In many instances, the approximate orbital parameters of an object are known from previous observation (either from the same or from a different instrument), and

follow-up observations are scheduled to update the parameters. This is particularly important for objects in low altitudes, where the residual atmosphere can have a noticeable, but hard to predict, impact on the flight path. Also, detailed, highly accurate follow-up observations are necessary if preliminary data from survey observations indicate a possible risk of conjunction. Both these scenarios, and especially their combination, can be a prime objective for the use of laser ranging (see also section 2.2).

Currently, the popular two-line elements (TLE) are used for tracking objects in our experiment, but predictions using other orbital parameter sets can be implemented easily in the software. It turns out, however, that the accuracy of the TLE data is usually good enough to detect the object in the large field of view of the current set-up. Nevertheless, the object is often not very well centred in the image, and may even gradually drift out of the field of view during the tracking. To improve this situation, a closed loop control has been implemented, which corrects possible deviations between the actual object position and the telescope pointing.

4.4 Tracking objects without known orbital parameters

For the discovery of debris particles which are not yet catalogued or appear far away from their expected path, the system must be able to discover new objects by itself. For this, the system is set to a fixed position in the sky, usually at rather low altitude angles, and takes images continuously. The most promising viewing directions and the expected number of detections are given in [15]. To catch as many objects as possible, the images should be taken with as little dead time in between as possible. For our current system, the read-out of the camera data to the computer poses the bottleneck that limits the image rate. Using a rather coarse binning, e.g. three to five, proves to be beneficial for these observations for two reasons: First, the data transfer can be sped up by more than an order of magnitude, second it results in more light per pixel generated by an object flying through the field of view. With a binning of three, images can be taken about every three seconds in the current configuration (FLI camera). With the Andor camera, on the other hand, it will be possible to record many images per second.

To 'capture' an object and to start tracking, each image must be inspected automatically directly after the exposure. If an arc is found, its position, length and direction are extracted and used to predict the object's apparent flight path for the next few seconds. It has been found that the assumption of a linear path is sufficient for this task [14]. In leap-frog tracking mode, the telescope slews to a position a few seconds ahead and takes an image at the predicted time of arrival. In

continuous tracking, the telescope starts moving into the predicted direction with an velocity inferred from the track length.

Again, this operation is complicated by the ambiguity of the track direction, i.e. the telescope may start tracking exactly opposite of the correct direction. If the object appears in two subsequent images taken from the same position, this problem can be remedied. At low altitude angles, this is usually possible due to the relatively low angular velocity of the object.

5 FIRST RESULTS

5.1 Operational parameters

From April to July 2013, the system has been used for observations in about 20 nights. The main reasons for loss of observation time are cloudy skies, followed by conflicting duties of the operators. The observations have been used to rate and optimise the system performance and to gather information about the environmental parameters. Additionally, several objects in LEO with known orbital parameters have been tracked successfully in leap-frog mode.

5.2 Environmental data

In various runs the telescope has been pointed to single, bright stars for periods of ten up to thirty minutes. Images have been taken continuously and the exact position of the star has been determined by fitting a Gaussian distribution. The displacement of the star in between images is in part due to turbulences in the atmosphere (fast changes), in part due to imperfections of the telescope tracking (slower changes). In figure 5, one example of such a run is shown. If the low frequency changes due to the telescope tracking are subtracted, the remaining fast jitter is in the order of 1 arcsecond (1 sigma, along one image axis). The seeing, i.e. the displacement due to air turbulences, is calculated from the total displacement in both axes, and amounts to about 1.5 arcseconds in this example. In various runs, similar measurements have been taken with different pointings in azimuth (towards the grasslands in the hills versus towards the city centre) and altitude. Overall, the seeing is found to be in the order of 1.1 to 1.8 arcseconds, which is a reasonable result.

To measure the light pollution, the procedure described in [3] is used. The first preliminary results indicate that the night sky brightness in the B band is around 19 mag / arcsec² (depending on the viewing direction).

During the course of the project, these and other environmental parameters (percentage of cloudless

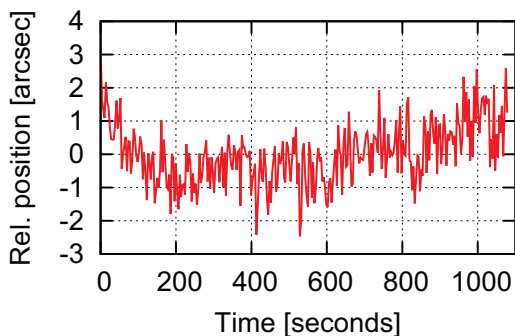


Figure 5: Position of the centre of the star Vindemiatrix (mag = 2.85) along one axis in the image. During the observations, the star appeared at altitudes of 21 to 24 degrees above the horizon. The deviations from nominal position are due to seeing and tracking inaccuracies.

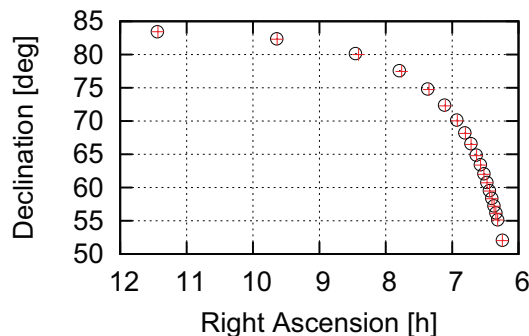


Figure 7: Trajectory of Envisat as observed during a pass at 2013-07-12 around 20:44 UTC. The black open circles denote the position predicted by TLE data, the red crosses show the measured position. Only half of the measured trajectory is shown for better visibility.

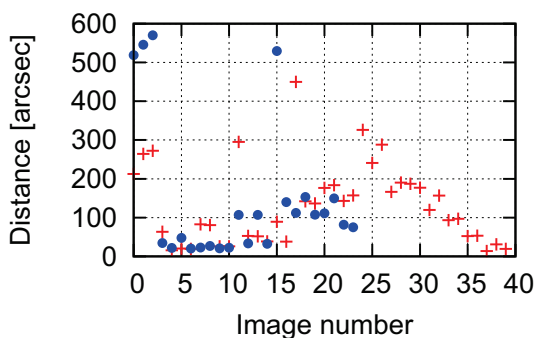


Figure 6: Distance of tracked object (middle of trail) from camera centre for observed passes of satellites Spot 5 (2013-07-07, red crosses) and IRS-P4 (2013-07-11, blue circles).

nights, extinction, etc.) will be measured in more detail.

5.3 System performance

After establishing a first pointing model, the free blind pointing accuracy of the telescope was tested on about forty bright stars and found to be in the order of 25 arcseconds (1 sigma). It is expected that this value will improve towards the nominal five arcseconds upon creation of a more accurate pointing model. The medium term tracking accuracy (10 minutes) for stars is in the order of one arcsecond, as stated by the mount manufacturer (see also figure 5).

The telescope can reach an arbitrary position in the sky in about ten to thirty seconds (the times around thirty seconds are usually due to a pier flip). During tracking of orbital objects, a new telescope position is usually reached and stabilised within three seconds.

Using the closed loop feature, tracked orbital ob-

jects are usually captured within one to three arcminutes from the camera centre. Figure 6 shows the distance of the track from the camera centre for two tracked objects. The improvement achieved by the closed loop feature, which is enabled after three images, is clearly visible.

The main reason for the remaining offset is the jitter of the camera trigger: So far, the camera is software triggered by the PC over an USB interface, and the time difference between the nominal start of exposure and the actual opening of the shutter is not well defined. Currently, upgrades to overcome this problem are being designed.

In continuous tracking mode, this time jitter is however not impeding the closed loop tracking, and it is therefore expected that even with the current camera system a much more accurate tracking can be achieved there. Unfortunately, not enough data could be gathered yet to evaluate this.

5.4 Observed objects

In table 4, a selection of so-far tracked objects is shown along with the amount of data recorded. All observations presented here have made use of leap-frog tracking. Typically, around 20 to 50 images can be recorded in the case of successful tracking. The smallest objects tracked so far have been the DLR-Tubsat and the Turkish earth observation satellite RASAT. The observation of smaller objects is impeded mainly by the night sky brightness at the observatory site. In leap-frog mode, the object remains only a few milliseconds on each camera pixel, therefore short exposure times and large binnings must be used for small, faint orbital objects.

Figures 7 to 9 show typical examples of data gathered during a satellite pass, in this case for the ob-

Name	Date	Images	Duration	Size (m)
Alos Daichi	06-08	39	7:00	4.5 x 6.5 x 28
Envisat	06-18	20	3:30	4.5 x 10 x 26
	07-12	53	9:30	
Rapideye 3	07-07	10	3:00	0.8 x 0.8 x 0.8
RASAT	07-12	20	5:00	0.6 x 0.6 x 0.6
DLR-Tubsat	07-12	10	1:00	0.4 x 0.6 x 0.6

Table 4: Collected data of tracked objects (selection). Dates are in month / day and all in the year 2013. The size given in the last column is taken from DISCOS [10] and indicative only.

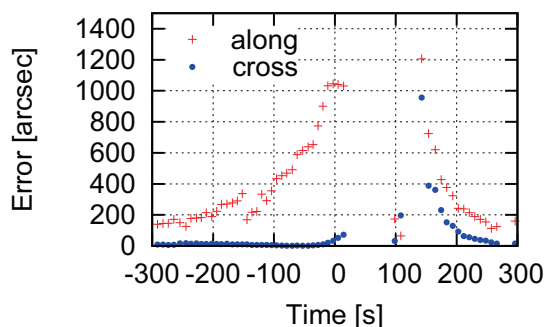


Figure 8: The cross-track and along-track errors measured during the pass of Envisat on 2013-07-12.

servation of Envisat on July 12th, 2013 from 20:39 to 20:49 UTC. In figure 7, the measured orbital positions are shown in comparison to the positions expected from TLE data from Celestrak [8]. To derive the observed object position with high precision, the pointing of the telescope is not inferred from the nominal pointing of the mount, but from the position of the stars visible in the field of view². While prediction and observation agree quite well, a small deviation along the track is already visible in this plot.

The deviations between predicted and observed position are plotted in detail in figure 8. They are split up into the components parallel (along) and perpendicular (cross) to the predicted track. Several features can be seen here: First, both errors increase towards the middle of the observation, where the object has reached its highest altitude (about 83° in this case) and thus its highest angular velocity. Especially the along track error, which is caused mainly by the delay between the PC trigger signal and the actual start of exposure, increases significantly due to the increased angular velocity. The cross track error, on the other hand, is not affected by the camera trigger delay and is therefore much smaller. During the ascension, it is well below 50 arcseconds. After the meridian pass of the object, and the resulting pier flip of the telescope (which also causes the gap in the data), the cross track error reaches values of up to about one

²Using the software package Pinpoint, <http://pinpoint.dc3.com/>

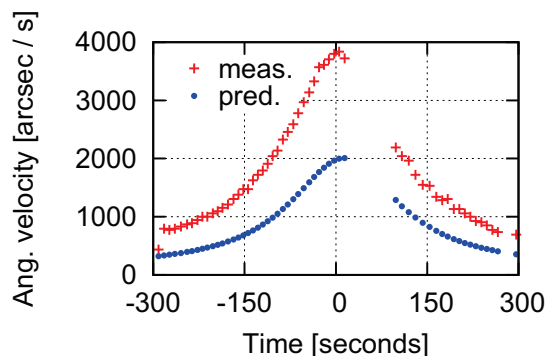


Figure 9: Angular velocity of Envisat as observed during the pass at 2013-07-12. The measured angular velocity (red crosses) is derived from the track length and the nominal exposure time of the camera (here: 0.1 seconds). The predicted angular velocity (blue dots) is derived from TLE data.

arcminute. The reason for this is not yet understood. During the descent, both errors decrease to the values observed during the start of the observation.

While the errors recorded here are largely due to inaccuracies of the current experimental set-up, it should be noted that the prediction based on public TLE data is also not perfect. Once the known issues impeding the accuracy are solved, it is planned to evaluate and further refine the instrument accuracy using more precise orbital data obtained e.g. by SLR stations or from the satellite operators.

Figure 9 shows the angular velocity of the object as inferred from the track length in the images along with the prediction from TLE data. While the shape of predicted and observed velocities agree very well, there is a significant systematic offset between the two. The reason for this offset seems to be that the camera shutter remains open beyond the nominal exposure time. Indications for this behaviour have also been found in other, independent measurements (e.g. recorded star brightness versus exposure time). From the smoothness of the observed data curve it is anticipated that the deviation of the exposure time is rather constant. It is therefore expected that the offset can be compensated for once it is accurately measured and characterised.

6 SUMMARY AND OUTLOOK

In this paper, the current status of the space debris observations in Stuttgart have been presented. A first version of the set-up has been used for test observations from April 2013 to July 2013, and some early results concerning the instrumental performance have been presented. In the near future, the system will be further upgraded and characterised with the goal to allow precise passive-optical tracking of large space debris objects. On the one hand this can be used to evaluate and demonstrate the potential of pure passive optical observations of space debris in LEO. On the other hand this system will be the cornerstone for the development of an active observation channel using laser ranging, which requires detection and accurate tracking of orbital objects by passive optical means. It is anticipated that the development and set-up of the active channel can start in 2014 with first results in early 2015.

7 Acknowledgements

The authors would like to thank the technical staff at DLR and the volunteers at the Stuttgart Observatory for their great support during installation and operation of the system.

References

- [1] Andor. iXon Ultra 897. http://www.andor.com/pdfs/specifications/Andor_iXon_Ultra_897_Specifications.pdf. [Online; accessed 26-June-2013].
- [2] Astelco website. <http://www.astelco.com/>. [Online; accessed 26-June-2013].
- [3] F. Falchi. Campaign of sky brightness and extinction measurements using a portable ccd camera. *Monthly Notices of the Royal Astronomical Society*, 412(1):33–48, 2011.
- [4] Finger Lakes Instruments. ProLine 16083 data sheet. http://www.flicamera.com/spec_sheets/PL16803.pdf. [Online; accessed 26-June-2013].
- [5] A. Giesen and J. Speiser. High-power thin disk lasers. In *Proc. SPIE 8547, High-Power Lasers*, 2012.
- [6] B. Greene, Y. Gao, C. Moore, et al. Laser tracking of space debris. In *Proceedings of 13th Laser Ranging Workshop*, 2002.
- [7] W. Hausleitner, G. Kirchner, S. Krauss, et al. Improved kHz-SLR tracking techniques and orbit quality analysis for LEO missions. *Advances in Space Research*, 45:721–732, March 2010.
- [8] T. S. Kelso. SATCAT. <http://celestrak.com/satcat/>, 2013. [Online; accessed 25-June-2013].
- [9] G. Kirchner, F. Koidl, F. Friederich, et al. Laser measurements to space debris from Graz SLR station. *Advances in Space Research*, 51:21–24, January 2013.
- [10] H. Klinkrad. DISCOS - ESA's database and information system characterising objects in space. *Advances in Space Research*, 11(12):43 – 52, 1991.
- [11] A. Milani, D. Farnocchia, L. Dimare, et al. Innovative observing strategy and orbit determination for Low Earth Orbit space debris. *Planet. Space Sci.*, 62:10–22, March 2012.
- [12] Orbital Debris Program Office. History of on-orbit satellite fragmentations 14th edition. 2008.
- [13] PlaneWave website. <http://planewave.com/products-page/telescopes/17-inch-cdk-optical-tube-assembly/>. [Online; accessed 26-June-2013].
- [14] J. Radtke. Visibility studies and orbit determination of space debris objects for a combined passive-optical and laser ranging station, 2012. Diploma thesis at Institute for Technical Physics of DLR, Stuttgart.
- [15] J. Radtke, I. Buske, U. Völker, et al. Visibility aspects of passive and active optical monitoring of space debris in low earth orbits. *DLRK 2012*, document id 281467, 2013.
- [16] E. Ryan and W. Ryan. The Magdalena Ridge Observatory's 2.4-meter Fast-Tracking Telescope: Space Situational Awareness and the Near-Earth Environment. In *Advanced Maui Optical and Space Surveillance Technologies Conference*, September 2011.
- [17] T. Schildknecht. Optical surveys for space debris. *The Astronomy and Astrophysics Review*, 14(1):41–111, 2007.
- [18] H. R. Schmitt, R. B. Hindsley, J. T. Armstrong, and E. K. Baines. Precise altitude measurements of LEO objects with simultaneous observations by multiple telescopes. In *Society of Photo-Optical Instrumentation Engineers (SPIE) Conference Series*, volume 8385 of *Society of Photo-Optical Instrumentation Engineers (SPIE) Conference Series*, May 2012.

- [19] C. Smith. The EOS Space Debris Tracking System. *AMOS Conf. Techn. Papers*, 2006.
- [20] U. Voelker, I. Buske, Th. Hall, et al. Laser-based space debris monitoring. In *Cambridge AIP Conf. Proc.*, page 354.
- [21] U. Völker, F. Friederich, I. Buske, et al. Laser based observation of space debris: Taking benefits from the fundamental wave. In *Proc. of 6th european conference on space debris*, 2013.
- [22] C. Wiedemann, S. K. Flegel, M. Moeckel, et al. The space debris environment model master-2009. *28th International Symposium on Space Technology and Science (ISTS)*, 2011.
- [23] Z.-P. Zhang, F.-M. Yang, H.-F. Zhang, et al. The use of laser ranging to measure space debris. *Research in Astronomy and Astrophysics*, 12:212–218, February 2012.